Geophysical and Astrophysical Fluid Dynamics
Vol. 00, No. 00, 00 Month 2023, 1–22

Baroclinic instability in a coupled oceanic-atmospheric Eady model

Armand VIC†*, Xavier CARTON † and Jonathan GULA †‡

† Univ Brest, CNRS, Ifremer, IRD, Laboratoire d'Océanographie Physique et Spatiale (LOPS), IUEM, 29280, Plouzané, France.
‡ Institut Universitaire de France (IUF), Paris, France

(*v4.4 released October 2012*)

The linear instability of coupled atmospheric and oceanic flows is studied theoretically. These flows are a westerly wind thermally or mechanically coupled to a westerly ocean current. In each fluid, a two-level surface quasi-geostrophic model is used to calculate the evolution of the initially perturbed flow. Each perturbation is a normal mode disturbance in streamfunction. Typical values of atmospheric and oceanic parameters are used for the models. Firstly, the models are not coupled and the flow instability in each fluid is validated separately against the results of the Eady model of baroclinic instability. Instability occurs at longer wavelengths in the atmosphere than in the ocean. Secondly, the ocean and atmosphere are thermally or mechanically coupled. With thermal coupling, instability decreases in the atmosphere; in the ocean, the coupling favors very long unstable waves, while shorter waves become less unstable. With respect to the meridional wavelengths of the perturbation, wider waves remain more unstable than narrower waves in the presence of thermal coupling. When the thermal coupling is increased further, both flow instabilities are damped. Also, the effect of the thermal coupling is more pronounced on the ocean when the oceanic flow has a small vertical shear of velocity. The mechanical coupling has a weak effect on the instability of the coupled system; this is explained by the phase shifts of the perturbations. This study is a first step towards studying more realistic cases.

Keywords: mathematical model, surface quasi-geostrophy, flow instability, stratified rotating flow, atmosphere-ocean coupling, linearized equations, baroclinic instability, Eady model, growth rates.

1. Introduction

Planetary-scale atmospheric and oceanic flows are driven by a geographic imbalance between the primary sources and sinks of heat. These two fluids gain more heat at the equator and lose more heat at the poles. As a result, atmospheric winds and oceanic currents transport heat meridionally (from south to north in the northern hemisphere) (Bjerkness 1966, Fofonoff 1981). More generally, heat is transported in the atmosphere and oceans by several processes : currents, nonlinear waves, and vortices (Richardson 1983, Carton 2010). These processes have different time and space scales and they interact non-linearly within each fluid (Fernández-Castro *et al.* 2020, Vic *et al.* 2021). The two fluids, the ocean and the atmosphere, also interact with each other on all scales and at all latitudes. Through these interactions, they exchange heat and momentum (McCreary 1983, Chelton and Xie 2010, Stevens *et al.* 2021).

Although the meridional flows are essential for planetary heat transfer, the strongest flows in the ocean and atmosphere are roughly zonal (east-west). In the atmosphere, these zonal flows are the main winds, generated by the deflection of the meridional air flows by the Coriolis force. In the oceans, they are the main surface currents due to the wind

*Corresponding author. Email: armand.vic@univ-brest.fr

forcing (Fofonoff 1981, Nowlin and Klinck 1986). These large-scale flows (on a scale of a few thousand kilometers) give rise to smaller-scale structures through instabilities. These smaller structures are the mesoscale waves and vortices, a few hundred kilometers in size (Carton 2001). Mesoscale flows, in turn, can become unstable, and produce submesoscale structures, with scales of a few kilometers (McWilliams 2016, Gula *et al.* 2022). Flow instabilities are therefore one of the processes by which energy is exchanged between scales within the ocean and the atmosphere (Holland and Haidvogel 1980, Tulloch *et al.* 2011, Duarte *et al.* 2011, Meunier *et al.* 2013, Duarte *et al.* 2016).

In the literature of ocean-atmosphere dynamics, many theoretical studies have been devoted to the response of oceanic motions to atmospheric forcing, or vice versa (one-way interactions). Less common are theoretical studies of coupled ocean-atmosphere dynamics (that is, with two-way interactions). Recently, the coupling of oceanic and atmospheric flows has been shown to affect ocean dynamics at the mesoscale or submesoscale (Renault *et al.* 2016, 2017, 2018). Therefore, the ocean-atmosphere dynamics with two-way interactions is clearly not the superposition of the two dynamics with one-way interactions; this is due to the nonlinearity of oceanic and atmospheric motions. The present theoretical study is devoted to understanding how the coupling of oceanic and atmospheric flows modifies *their instabilities*.

In the present study, we investigate how two unstable parallel flows, one in the atmosphere and one in the ocean, evolve linearly when they are coupled. We contrast the coupled flow instability with the uncoupled flow instability. Our westerly currents have a vertical shear of horizontal velocity, which is the basis for baroclinic instability on a rotating planet. The driver of baroclinic instability is the conversion of potential energy of the mean (westerly) current or wind, to the kinetic energy of the perturbation.

To study baroclinic instability of coupled westerly flows, we generalize the Eady model to an ocean coupled with an atmosphere (Eady 1949). In the original Eady model, only one fluid is considered. In this fluid, the flow is horizontally uniform, and vertically sheared. The mathematical equations governing the Eady model are derived from the surface quasi-geostrophic dynamics (Bretherton 1966, Held *et al.* 1995, Lapeyre 2017). In surface quasi-geostrophy, the potential vorticity is null in the interior of the fluid. The surface quasi-geostrophic equations represent the advection of buoyancy on the horizontal surfaces bounding the fluid (top and bottom surfaces).

To couple the atmosphere and the ocean, we propose two different way to model it. Adding a thermal relaxation at the ocean-atmosphere interface mimics a sensible heat flux proportional to the temperature difference between the two fluids is called "thermal coupling" in the rest of the article. We also investigate how a frictional stress between the two fluids influences the linear instabilities rather than the thermal relaxation. This kind of coupling is called "mechanical coupling" in the following. These formulations of the ocean-atmosphere coupling, which retain some physical realism, are simple enough to allow an analytical approach. The most unstable perturbations can be computed for the atmosphere and the ocean, globally, separately in each fluid or separately in each layer.

The paper is organized as follows: we present the physical model and the surface quasi-geostrophic (SQG) equations in section 2. In section 3, we calculate the linearized equations for the instability of thermally coupled westerly flows and we provide an asymptotic analytical solution. In section 4, these equations are solved numerically for the thermally coupled model. The results are validated against the Eady model solutions for uncoupled ocean and atmosphere (section 4.2). They are presented in the presence of thermal coupling for a ref-

erence case typical of atmospheric winds and of ocean currents (section 4.3). We conduct a sensitivity study of the instability growth rates and wavelengths to the physical parameters and the coupling strength (sections 4.4 and 4.5). In section 5, we detail the calculations and numerical results for the linear instability of mechanically coupled flows. The results are discussed (section 6) and a conclusion is given (section 7). In the appendix, we present the phase shift of the perturbation between consecutive levels.

2. Surface quasi-geostrophic model and equations

2.1. *Basic equations: the surface quasi-geostrophic model*

We use a simple mathematical model of fluid flows, able to represent the instability of westerly winds or currents, with vertical shear of velocity. This model is the SQG model. Quasi-geostrophy (QG) is an extension of the stationary geostrophic balance, to slowly changing dynamics, evolving close to this balance.

Firstly we consider a single fluid. For fluid flows with rapid planetary rotation and strong fluid stratification, the momentum equations are quasi two dimensional (horizontal):

$$\partial_t u + u\partial_x u + v\partial_y u - f_0 v = -(1/\rho_0)\partial_x p \tag{1a}$$

$$\partial_t v + u\partial_x v + v\partial_y v + f_0 u = -(1/\rho_0)\partial_y p \tag{1b}$$

where (u, v) are the zonal (east-west) and meridional (north-south) components of the velocity, p is pressure, ρ_0 is an average density of the fluid and f_0 is the Coriolis parameter: $f_0 = 2\Omega\sin(\theta)$, with Ω the rotation rate of the Earth and θ the latitude. The transport terms

$$\frac{\mathrm{D}}{\mathrm{D}t}(u, v) = [\partial_t + u\partial_x + v\partial_y](u, v) \tag{2}$$

are called the relative acceleration and $-f_0 v$, $f_0 u$ is the Coriolis acceleration. In the geostrophic balance, the relative acceleration is null. In the quasi-geostrophic model, the relative acceleration is weak compared to the Coriolis acceleration. The ratio of the former to the latter is the Rossby number $Ro = U/f_0 L$ which is small compared to unity. From the geostrophic balance, a streamfunction can be written from which the horizontal velocity derives at first order in Ro: $\psi = p/(\rho_0 f_0)$. We have $u \sim -\partial_y\psi, v \sim \partial_x\psi$. The key equation governing the quasi-geostrophic model is the conservation of potential vorticity in the absence of forcing and of dissipation.
It is written

$$\frac{\mathrm{D}q}{\mathrm{D}t} = 0, \quad q = \left[\partial_x^2 + \partial_y^2\right]\psi + \partial_z\left[\frac{f_0^2}{N^2}\partial_z\psi\right] \tag{3}$$

where N^2 is the Brunt Väisälä frequency: $N^2 = -(g/\rho_0)\ \partial\rho/\partial z$. This potential vorticity equation is obtained from the curl of the momentum equations and from the conservation of mass (Carton 2001).
When the potential vorticity is null in the bulk of the fluid and is concentrated at the surface and at the bottom (respectively top) of the ocean (respectively atmospheric boundary layer), we have

$$q = q_1\delta(z = 0) + q_2\delta(z = \pm H) \tag{4}$$

where δ is the Dirac distribution and H is the depth (or mixed layer depth) of the ocean or the height of the atmospheric boundary layer. The potential vorticity equations become the conservation of buoyancy anomaly b on these two surfaces.

$$\frac{\mathrm{D}b}{\mathrm{D}t} = 0 \quad \text{for } z = 0, \pm H \quad \text{and } b = f_0 \partial_z \psi \tag{5}$$

The latter two equations are the basis of the Eady model for the baroclinic instability of the atmosphere or the ocean. Note that b is a buoyancy anomaly with respect to the state of rest. At the interface between the two fluids, in the advection equation for buoyancy will appears a coupling term modelling the exchange of temperature (thermal coupling) or the friction between the two fluids (mechanical coupling).

2.2. *Basic equations : the four layer case*

Now, we consider a system with two coupled fluids: the atmosphere and the ocean. In the atmosphere ($z > 0$), the streamfunction is $\psi_\mathrm{a}(x, y, z, t)$. In the ocean ($z < 0$), it is $\psi_\mathrm{o}(x, y, z, t)$. The horizontal velocities are $u_a = -\partial_y \psi_a$, $v_a = \partial_x \psi_a$; $u_\mathrm{o} = -\partial_y \psi_\mathrm{o}$, $v_\mathrm{o} = \partial_x \psi_\mathrm{o}$.
Associated with these streamfunctions are buoyancy anomalies $b_\mathrm{o} = f_0 \partial_z \psi_\mathrm{o}$ (for the ocean) and $b_\mathrm{a} = f_0 \partial_z \psi_\mathrm{a}$ (for the atmosphere). The potential vorticity of the (oceanic, atmospheric) flow is

$$q_\mathrm{o} = \left[\partial_x^2 + \partial_y^2 + \left(\frac{f_0}{N_\mathrm{o}} \right)^2 \partial_z^2 \right] \psi_\mathrm{o} \tag{6a}$$

$$q_\mathrm{a} = \left[\partial_x^2 + \partial_y^2 + \left(\frac{f_0}{N_\mathrm{a}} \right)^2 \partial_z^2 \right] \psi_\mathrm{a} \tag{6b}$$

where N_o and N_a are the Brunt-Väisälä frequencies of the ocean and the atmosphere at rest. We call H_o and H_a the depth of the ocean and the height of the atmosphere. If one considers only the turbulent boundary layers, H_o and H_a are the depth of the ocean mixed layer or the height of the atmospheric boundary layer. Finally we call L_o and L_a the characteristic horizontal scales of motion in the ocean and in the atmosphere. We call (normalized) radii of deformation, the ratios $\sigma_\mathrm{o} = \frac{N_\mathrm{o} H_\mathrm{o}}{f_0 L_\mathrm{o}}$ in the ocean and $\sigma_\mathrm{a} = \frac{N_\mathrm{a} H_\mathrm{a}}{f_0 L_\mathrm{a}}$ in the atmosphere. Furthermore, the buoyancy frequencies in the lower atmosphere and in the upper ocean are quite similar; therefore, we will set $N_\mathrm{a} = N_\mathrm{o}$ for the rest of the study.

According to the hypotheses of the *surface* quasi-geostrophic model (Held *et al.* 1995, Lapeyre 2017, Carton 2009), the potential vorticity vanishes in the interior of each fluid

$$q_\mathrm{a} = \nabla_\mathrm{h}^2 \psi_\mathrm{a} + \frac{f_0^2}{N_\mathrm{a}^2} \partial_z^2 \psi_\mathrm{a} = 0 \quad \text{for} \quad 0 < z < H_\mathrm{a} \tag{7a}$$

$$q_\mathrm{o} = \nabla_\mathrm{h}^2 \psi_\mathrm{o} + \frac{f_0^2}{N_\mathrm{o}^2} \partial_z^2 \psi_\mathrm{o} = 0 \quad \text{for} \quad -H_\mathrm{o} < z < 0 \tag{7b}$$

At the upper and lower surfaces of each fluid (levels $1, 2, 3$ and 4: top and bottom of the atmosphere, top and bottom of the ocean), buoyancy plays the role of a Dirac function in z for the PV field:

$$f_0 \frac{\partial \psi_\mathrm{a}}{\partial z}\bigg|_{z=H_\mathrm{a}} = b_1 \quad , \quad f_0 \frac{\partial \psi_\mathrm{a}}{\partial z}\bigg|_{z=0} = b_2 \tag{8a}$$

$$f_0 \frac{\partial \psi_\mathrm{o}}{\partial z}\bigg|_{z=0} = b_3 \quad , \quad f_0 \frac{\partial \psi_\mathrm{o}}{\partial z}\bigg|_{z=-H_\mathrm{o}} = b_4. \tag{8b}$$

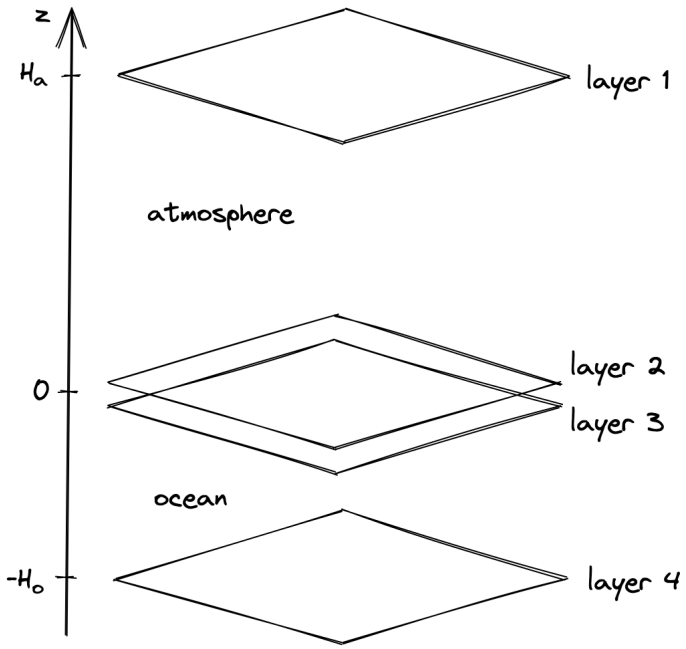

Figure 1. Sketch of the 4 layer surface quasi-geostrophic model; the coupling of the atmosphere with the ocean is achieved between levels 2 and 3.

3. Linear instability of the thermally coupled ocean-atmosphere flow: analytical results

When the atmosphere and ocean are thermally coupled, the buoyancies obey the following transport equations at each layers:

$$\frac{\mathrm{D}b_1}{\mathrm{D}t} = \frac{\mathrm{D}b_4}{\mathrm{D}t} = 0 \tag{9a}$$

$$\frac{\mathrm{D}b_2}{\mathrm{D}t} = C_\mathrm{o}(b_3 - b_2) + F_\mathrm{o} \tag{9b}$$

$$\frac{\mathrm{D}b_3}{\mathrm{D}t} = C_\mathrm{a}(b_2 - b_3) + F_\mathrm{a} \tag{9c}$$

where $C_\mathrm{o}, C_\mathrm{a}$ are the coupling coefficients (of the sensible heat flux between both fluids) and $F_\mathrm{o}, F_\mathrm{a}$ are the forcing terms (e.g. other thermal forcing) that allow a steady basic state. We note C_o the constant for the coupling term at level 2 because it represents the flux from the upper ocean to the lower atmosphere (and conversely for C_a at level 3). In our problem, we have chosen to study the instability of a steady state in two coupled fluids. This is a first step; the study of time-dependent coupled flows should be carried out in a sequel of this work.

3.1. *Basic state*

We choose two steady currents in the ocean and the atmosphere as a basic state; these currents flow in the East-West direction:

$$\Psi_\mathrm{a}(y,z) = -\Pi_\mathrm{a} y - \Lambda_\mathrm{a} yz \tag{10a}$$

$$\Psi_\mathrm{o}(y,z) = -\Pi_\mathrm{o} y - \Lambda_\mathrm{o} yz \tag{10b}$$

where Λ_a, Λ_o, Π_a and Π_o are positive constants. The horizontal mean flows in the ocean and the atmosphere depend only on z: the meridional velocities are null $V_\mathrm{a} = V_\mathrm{o} = 0$ and the zonal

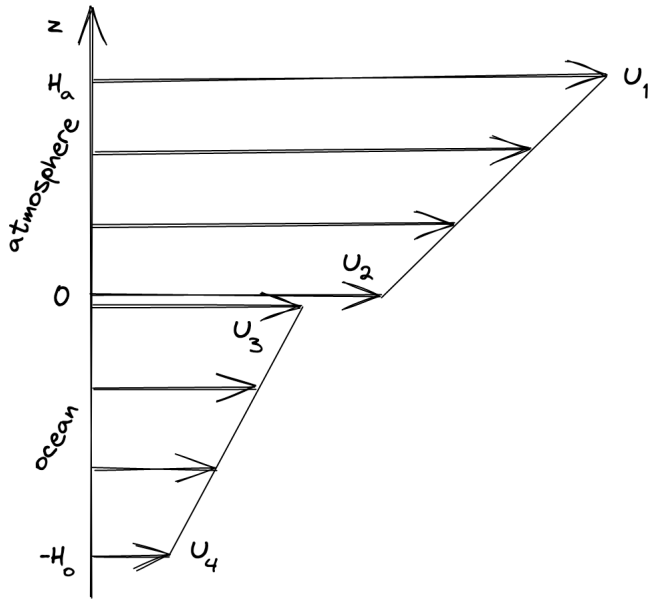

Figure 2. Zonal velocities of the basic state in the atmosphere and ocean

velocities are increasing with z, as shown in Figure 2 and computed here:

$$U_{\rm a}(z) = -\partial_y \Psi_{\rm a} = \Lambda_{\rm a} z + \Pi_{\rm a} \tag{11a}$$

$$U_{\rm o}(z) = -\partial_y \Psi_{\rm o} = \Lambda_{\rm o} z + \Pi_{\rm o} \tag{11b}$$

or at each level:

$$U_1 = \Pi_{\rm a} + \Lambda_{\rm a} H_{\rm a}, \quad U_2 = \Pi_{\rm a}, \quad U_3 = \Pi_{\rm o}, \quad U_4 = \Pi_{\rm o} - \Lambda_{\rm o} H_{\rm o} \tag{12}$$

The steady buoyancies in the four layers are:

$$B_1 = B_2 = -f_0 \Lambda_{\rm a} y \tag{13a}$$

$$B_3 = B_4 = -f_0 \Lambda_{\rm o} y \tag{13b}$$

It is a steady basic state because it satisfies equations (7) and obviously $\frac{{\rm D}B_1}{{\rm D}t} = \frac{{\rm D}B_4}{{\rm D}t} = 0$. The two transport equations for the atmospheric and oceanic mean flows at the interface (equations (9b) and (9c)) must satisfy:

$$\frac{{\rm D}B_2}{{\rm D}t} = C_{\rm o}(B_3 - B_2) + F_{\rm o} = f_0 C_{\rm o} y(-\Lambda_{\rm o} + \Lambda_{\rm a}) + F_{\rm o} \tag{14a}$$

$$\frac{{\rm D}B_3}{{\rm D}t} = C_{\rm a}(B_2 - B_3) + F_{\rm a} = f_0 C_{\rm a} y(-\Lambda_{\rm a} + \Lambda_{\rm o}) + F_{\rm a} \tag{14b}$$

and both right hand sides must vanish for stationarity. Therefore the forcings $F_{\rm o}$ and $F_{\rm a}$ are:

$$F_{\rm o} = -f_0 C_{\rm o} y(\Lambda_{\rm a} - \Lambda_{\rm o}) \tag{15a}$$

$$F_{\rm a} = f_0 C_{\rm a} y(\Lambda_{\rm a} - \Lambda_{\rm o}) \tag{15b}$$

to make the basic state stationary. Obviously, in the absence of other forcing, the mean buoyancy would tend to equate at levels 2 and 3 on the long run.

3.2. *Perturbations*

The flow is now perturbed by a normal mode disturbance in each fluid. The total streamfunctions are:

$$\psi_{\rm o} = \Psi_{\rm o} + \psi'_{\rm o} \tag{16a}$$

$$\psi_{\rm a} = \Psi_{\rm a} + \psi'_{\rm a} \tag{16b}$$

and the associated buoyancies $b_i = B_i + b'_i$ in the four layers $i = 1, 2, 3, 4$ where we assume that the buoyancy perturbations in each layer are planar normal modes and are written as:

$$b'_i = \beta_i \, {\rm e}^{{\rm i}(kx+ly-\omega t)} \tag{17}$$

such that

$$\psi'_j = \varphi_j(z) \, {\rm e}^{{\rm i}(kx+ly-\omega t)} \tag{18a}$$

$$v'_j = \frac{\partial \psi'_j}{\partial x} = {\rm i}k\varphi_j(z) \, {\rm e}^{{\rm i}(kx+ly-\omega t)} \tag{18b}$$

for $j = {\rm a}, {\rm o}$ and φ_j functions of $\beta_1, \beta_2, \beta_3, \beta_4$: from equations (7) we get:

$$-\left(k^2 + l^2\right)\varphi_j + \frac{f_0^2}{N_j^2}\partial_z^2 \varphi_j = 0. \tag{19}$$

Then, if we set $K^2 = k^2 + l^2$, we can write solutions as:

$$\varphi_{\rm a}(z) = \lambda_{\rm a} \cosh\left(\frac{N_{\rm a}}{f_0} K z\right) + \mu_{\rm a} \cosh\left(\frac{N_{\rm a}}{f_0} K (z - H_{\rm a})\right) \tag{20a}$$

$$\varphi_{\rm o}(z) = \lambda_{\rm o} \cosh\left(\frac{N_{\rm o}}{f_0} K z\right) + \mu_{\rm o} \cosh\left(\frac{N_{\rm o}}{f_0} K (z + H_{\rm o})\right), \tag{20b}$$

where λ_j, μ_j are constants computed from boundary conditions (8):

$$\lambda_{\rm a} = \frac{\beta_1}{s_{\rm a}}, \quad \mu_{\rm a} = -\frac{\beta_2}{s_{\rm a}} \tag{21a}$$

$$\lambda_{\rm o} = -\frac{\beta_4}{s_{\rm o}}, \quad \mu_{\rm o} = \frac{\beta_3}{s_{\rm o}} \tag{21b}$$

where $s_{\rm a} = N_{\rm a} K \sinh\left(\frac{N_{\rm a}}{f_0} K H_{\rm a}\right)$, $t_{\rm a} = N_{\rm a} K \tanh\left(\frac{N_{\rm a}}{f_0} K H_{\rm a}\right)$, $s_{\rm o} = N_{\rm o} K \sinh\left(\frac{N_{\rm o}}{f_0} K H_{\rm o}\right)$, and $t_{\rm o} = N_{\rm o} K \tanh\left(\frac{N_{\rm o}}{f_0} K H_{\rm o}\right)$.

We now expand the buoyancies transport equations (9) at first order for the four layers; the left-hand side is:

$$\frac{{\rm D}b_i}{{\rm D}t} = \frac{\partial b'_i}{\partial t} + U_i \frac{\partial b'_i}{\partial x} + v'_i \frac{\partial B_i}{\partial y} \tag{22}$$

and the right-hand side is coupled for the interface layers $i = 1, 2$ and 0 for the two other layers $i = 1, 4$:

1^{st} *layer:*

$$-{\rm i}\omega\beta_1 + \left(\Pi_{\rm a} + \Lambda_{\rm a} H_{\rm a}\right) {\rm i}k\beta_1 - f_0 {\rm i}k\Lambda_{\rm a}\varphi_{\rm a}(z = H_{\rm a}) = 0 \tag{23}$$

but

$$\varphi_{\rm a}(z = H_{\rm a}) = \lambda_{\rm a} \cosh\left(\frac{N_{\rm a}}{f_0} K H_{\rm a}\right) + \mu_a = \frac{\beta_1}{t_{\rm a}} - \frac{\beta_2}{s_{\rm a}} \tag{24}$$

so

$$\left[\omega - k\left(\Pi_\mathrm{a} + \Lambda_\mathrm{a}\left(H_\mathrm{a} - \frac{f_0}{t_\mathrm{a}}\right)\right)\right]\beta_1 - \frac{f_0 k\Lambda_\mathrm{a}}{s_\mathrm{a}}\beta_2 = 0 \tag{25}$$

2^{nd} layer:

$$-\mathrm{i}\omega\beta_2 + \Pi_\mathrm{a}\mathrm{i}k\beta_2 - f_0\mathrm{i}k\Lambda_\mathrm{a}\varphi_\mathrm{a}(z=0) = C_\mathrm{o}\left(\beta_3 - \beta_2\right) \tag{26}$$

but

$$\varphi_\mathrm{a}(z=0) = \lambda_\mathrm{a} + \mu_\mathrm{a}\cosh\left(\frac{N_\mathrm{a}}{f_0}KH_\mathrm{a}\right) = \frac{\beta_1}{s_\mathrm{a}} - \frac{\beta_2}{t_\mathrm{a}} \tag{27}$$

so

$$\frac{f_0 k\Lambda_\mathrm{a}}{s_\mathrm{a}}\beta_1 + \left[\omega - k\left(\Pi_\mathrm{a} + \frac{f_0\Lambda_\mathrm{a}}{t_\mathrm{a}}\right) + \mathrm{i}C_\mathrm{o}\right]\beta_2 - \mathrm{i}C_\mathrm{o}\beta_3 = 0 \tag{28}$$

3^{rd} layer:

$$-\mathrm{i}\omega\beta_3 + \Pi_\mathrm{o}\mathrm{i}k\beta_3 - f_0\mathrm{i}k\Lambda_\mathrm{o}\varphi_\mathrm{o}(z=0) = C_\mathrm{a}\left(\beta_2 - \beta_3\right) \tag{29}$$

but

$$\varphi_\mathrm{o}(z=0) = \lambda_\mathrm{o} + \mu_\mathrm{o}\cosh\left(\frac{N_\mathrm{o}}{f_0}KH_\mathrm{o}\right) = \frac{\beta_3}{t_\mathrm{o}} - \frac{\beta_4}{s_\mathrm{o}} \tag{30}$$

so

$$-\mathrm{i}C_\mathrm{a}\beta_2 + \left[\omega - k\left(\Pi_\mathrm{o} - \frac{\Lambda_\mathrm{o}f_0}{t_\mathrm{o}}\right) + \mathrm{i}C_\mathrm{a}\right]\beta_3 - \frac{kf_0\Lambda_\mathrm{o}}{s_\mathrm{o}}\beta_4 = 0 \tag{31}$$

4^{th} layer:

$$-\mathrm{i}\omega\beta_4 + \left(\Pi_\mathrm{o} - \Lambda_\mathrm{o}H_\mathrm{o}\right)\mathrm{i}k\beta_4 - f_0\mathrm{i}k\Lambda_\mathrm{o}\varphi_\mathrm{o}(z=-H_\mathrm{o}) = 0 \tag{32}$$

but

$$\varphi_\mathrm{o}(z=-H_\mathrm{o}) = \lambda_\mathrm{o}\cosh\left(\frac{N_\mathrm{o}}{f_0}KH_\mathrm{o}\right) + \mu_o = \frac{\beta_3}{s_\mathrm{o}} - \frac{\beta_4}{t_\mathrm{o}} \tag{33}$$

so

$$\frac{f_0 k\Lambda_\mathrm{o}}{s_\mathrm{o}}\beta_3 + \left[\omega - k\left(\Pi_\mathrm{o} + \Lambda_\mathrm{o}\left(\frac{f_0}{t_\mathrm{o}} - H_\mathrm{o}\right)\right)\right]\beta_4 = 0 \tag{34}$$

The four dispersion relations (25), (28), (31) and (34) can be written in a matrix way: $\mathcal{M}\beta = 0$, where $\beta = \begin{pmatrix}\beta_1\\ \beta_2\\ \beta_3\\ \beta_4\end{pmatrix}$ and

$$\mathcal{M} = \begin{pmatrix} \omega - k\left(\Pi_\mathrm{a} + \Lambda_\mathrm{a}\left(H_\mathrm{a} - \frac{f_0}{t_\mathrm{a}}\right)\right) & \frac{-f_0 k\Lambda_\mathrm{a}}{s_\mathrm{a}} & 0 & 0 \\ \frac{f_0 k\Lambda_\mathrm{a}}{s_\mathrm{a}} & \omega - k\left(\Pi_a + \frac{f_0\Lambda_\mathrm{a}}{t_\mathrm{a}}\right) + \mathrm{i}C_\mathrm{o} & -\mathrm{i}C_\mathrm{o} & 0 \\ 0 & -\mathrm{i}C_\mathrm{a} & \omega - k\left(\Pi_\mathrm{o} - \frac{f_0\Lambda_\mathrm{o}}{t_\mathrm{o}}\right) + \mathrm{i}C_\mathrm{a} & -\frac{f_0 k\Lambda_\mathrm{o}}{s_\mathrm{o}} \\ 0 & 0 & \frac{f_0 k\Lambda_\mathrm{o}}{s_\mathrm{o}} & \omega - k\left(\Pi_\mathrm{o} + \Lambda_\mathrm{o}\left(\frac{f_0}{t_\mathrm{o}} - H_\mathrm{o}\right)\right) \end{pmatrix} \tag{35}$$

We want a non trivial solution of the equation $\mathcal{M}\beta = 0$. This means that $\det(\mathcal{M})$ should vanish. Analytically, $\det(\mathcal{M})$ can be computed but we failed to find simple analytical solutions in ω:

$$
\begin{aligned}
\det(\mathcal{M}) = &\left[\omega - k\left(\Pi_\mathrm{a} + \Lambda_\mathrm{a}\left(H_\mathrm{a} - \frac{f_0}{t_\mathrm{a}}\right)\right)\right]\left[\omega - k\left(\Pi_\mathrm{o} + \Lambda_\mathrm{o}\left(\frac{f_0}{t_\mathrm{o}} - H_\mathrm{o}\right)\right)\right] \\
&\left[\omega - k\left(\Pi_a + \frac{f_0\Lambda_\mathrm{a}}{t_\mathrm{a}}\right) + \mathrm{i}C_\mathrm{o}\right]\left[\omega - k\left(\Pi_\mathrm{o} - \frac{f_0\Lambda_\mathrm{o}}{t_\mathrm{o}}\right) + \mathrm{i}C_\mathrm{a}\right] \\
&+ \frac{f_0^2k^2\Lambda_\mathrm{o}^2}{s_\mathrm{o}^2}\left[\omega - k\left(\Pi_\mathrm{a} + \Lambda_\mathrm{a}\left(H_\mathrm{a} - \frac{f_0}{t_\mathrm{a}}\right)\right)\right]\left[\omega - k\left(\Pi_a + \frac{f_0\Lambda_\mathrm{a}}{t_\mathrm{a}}\right) + \mathrm{i}C_\mathrm{o}\right] \\
&+ \frac{f_0^2k^2\Lambda_\mathrm{a}^2}{s_\mathrm{a}^2}\left[\omega - k\left(\Pi_\mathrm{o} + \Lambda_\mathrm{o}\left(\frac{f_0}{t_\mathrm{o}} - H_\mathrm{o}\right)\right)\right]\left[\omega - k\left(\Pi_\mathrm{o} - \frac{f_0\Lambda_\mathrm{o}}{t_\mathrm{o}}\right) + \mathrm{i}C_\mathrm{a}\right] \\
&+ C_\mathrm{o}C_\mathrm{a}\left[\omega - k\left(\Pi_\mathrm{a} + \Lambda_\mathrm{a}\left(H_\mathrm{a} - \frac{f_0}{t_\mathrm{a}}\right)\right)\right]\left[\omega - k\left(\Pi_\mathrm{o} + \Lambda_\mathrm{o}\left(\frac{f_0}{t_\mathrm{o}} - H_\mathrm{o}\right)\right)\right] \\
&+ \frac{f_0^4k^4\Lambda_\mathrm{a}^2\Lambda_\mathrm{o}^2}{s_\mathrm{a}^2s_\mathrm{o}^2}
\end{aligned}
$$

$$
\begin{aligned}
\det(\mathcal{M}) = &\omega^4 - \omega^3(\delta_1 + \delta_2 + \delta_3 + \delta_4) \\
&+ \omega^2(A + B + C + \delta_1\delta_2 + \delta_1\delta_3 + \delta_1\delta_4 + \delta_2\delta_3 + \delta_2\delta_4 + \delta_3\delta_4) \\
&- \omega(A(\delta_1 + \delta_2) + B(\delta_3 + \delta_4) + C(\delta_1 + \delta_4) + \delta_1\delta_2\delta_3 + \delta_1\delta_2\delta_4 + \delta_1\delta_3\delta_4 + \delta_2\delta_3\delta_4) \\
&+ D + A\delta_1\delta_2 + B\delta_3\delta_4 + C\delta_1\delta_4 + \delta_1\delta_2\delta_3\delta_4
\end{aligned}
$$

where $\delta_1 = k\left(\Pi_\mathrm{a} + \Lambda_\mathrm{a}\left(H_\mathrm{a} - \frac{f_0}{t_\mathrm{a}}\right)\right)$, $\delta_2 = k\left(\Pi_\mathrm{a} + \frac{f_0\Lambda_\mathrm{a}}{t_\mathrm{a}}\right) - \mathrm{i}C_\mathrm{o}$, $\delta_3 = k\left(\Pi_\mathrm{o} - \frac{f_0\Lambda_\mathrm{o}}{t_\mathrm{o}}\right) - \mathrm{i}C_\mathrm{a}$, $\delta_4 = k\left(\Pi_\mathrm{o} + \Lambda_\mathrm{o}\left(\frac{f_0}{t_\mathrm{o}} - H_\mathrm{o}\right)\right)$ are the diagonal coefficient of the following matrix $\mathcal{A}$ defined in (38) and $A = \frac{f_0^2k^2\Lambda_\mathrm{o}^2}{s_\mathrm{o}^2}$, $B = \frac{f_0^2k^2\Lambda_\mathrm{a}^2}{s_\mathrm{a}^2}$, $C = C_\mathrm{o}C_\mathrm{a}$, $D = \frac{f_0^4k^4\Lambda_\mathrm{o}^2\Lambda_\mathrm{a}^2}{s_\mathrm{o}^2s_\mathrm{a}^2} = AB$.

3.3. *Limit for long zonal waves $k \to 0$ or very short waves $k \gg 1$ and finite width perturbations $l \neq 0$*

The determinant can easily be computed for long zonal waves $k \to 0$ with finite meridional scale $l \neq 0$: the matrix $\mathcal{M}$ becomes

$$
\lim_{k\to 0}\mathcal{M} = \begin{pmatrix} \omega & 0 & 0 & 0 \\ 0 & \omega + \mathrm{i}C_\mathrm{o} & -\mathrm{i}C_\mathrm{o} & 0 \\ 0 & -\mathrm{i}C_\mathrm{a} & \omega + \mathrm{i}C_\mathrm{a} & 0 \\ 0 & 0 & 0 & \omega \end{pmatrix} \tag{36}
$$

and the only non-real solution in ω for $\det \lim_{k\to 0}$ is:

$$
-\mathrm{i}[C_\mathrm{o} + C_\mathrm{a}] < 0 \tag{37}
$$

This solution can easily be obtained by considering a null mean flow (the mean flow terms are multiplied by ik), and by substracting the two linearized equations for the lower level of the atmosphere and for the upper level of the ocean. We obtain $\partial_t(b_2' - b_3') = -(C_\mathrm{o} + C_\mathrm{a})(b_2' - b_3')$. For very long wave perturbations, coupling leads to the damping of the difference between the lower atmospheric waves and the surface oceanic waves, as it will shown later in the numerical computation of the growth rates.

For very short waves $k \to \infty$, with finite l, the coupling becomes inefficient (the coupling coefficient is then iC/k in the linearized equations). We recover two independent Eady prob-

lems, one for the atmosphere and one for the ocean, which lead to stability in the short wave limit. The coupled system should therefore also be stable.

3.4. *Numerical approach*

Numerically, this problem is solved with eigenvalue routines; indeed $\mathcal{M} = \omega \mathrm{Id} - \mathcal{A}$. Solutions for ω such that $\det(\mathcal{M}) = 0$ are given by the eigenvalues of $\mathcal{A}$ with

$$\mathcal{A} = \begin{pmatrix} k\left(\Pi_\mathrm{a} + \Lambda_\mathrm{a}\left(H_\mathrm{a} - \frac{f_0}{t_\mathrm{a}}\right)\right) & \frac{f_0 k \Lambda_\mathrm{a}}{s_\mathrm{a}} & 0 & 0 \\ \frac{-f_0 k \Lambda_\mathrm{a}}{s_\mathrm{a}} & k\left(\Pi_\mathrm{a} + \frac{f_0 \Lambda_\mathrm{a}}{t_\mathrm{a}}\right) - \mathrm{i}C_\mathrm{o} & \mathrm{i}C_\mathrm{o} & 0 \\ 0 & \mathrm{i}C_\mathrm{a} & k\left(\Pi_\mathrm{o} - \frac{f_0 \Lambda_\mathrm{o}}{t_\mathrm{o}}\right) - \mathrm{i}C_\mathrm{a} & \frac{f_0 k \Lambda_\mathrm{o}}{s_\mathrm{o}} \\ 0 & 0 & \frac{-f_0 k \Lambda_\mathrm{o}}{s_\mathrm{o}} & k\left(\Pi_\mathrm{o} + \Lambda_\mathrm{o}\left(\frac{f_0}{t_\mathrm{o}} - H_\mathrm{o}\right)\right) \end{pmatrix} \tag{38}$$

The plotted quantities are defined as follows: p_a (resp. p_o) represents the sum of the atmospheric (resp. oceanic) growth rates of the instabilities, weighted by the magnitude of the eigenvectors in each fluid.

$$p_\mathrm{a} = \sum_{\substack{i=1 \\ \mathrm{Im}(\omega_i)>0}}^{4} \mathrm{Im}(\omega_i)\left(|x_{i,1}|^2 + |x_{i,2}|^2\right) \tag{39a}$$

$$p_\mathrm{o} = \sum_{\substack{i=1 \\ \mathrm{Im}(\omega_i)>0}}^{4} \mathrm{Im}(\omega_i)\left(|x_{i,3}|^2 + |x_{i,4}|^2\right) \tag{39b}$$

where $\{\omega_1, \omega_2, \omega_3, \omega_4\} = \mathrm{Sp}(\mathcal{A})$ are the eigenvalues of $\mathcal{A}$. $\{X_1, X_2, X_3, X_4\}$ is a set of normalized eigenvectors. For any $i = 1, 2, 3, 4$, $X_i = \begin{pmatrix} x_{i,1} \\ x_{i,2} \\ x_{i,3} \\ x_{i,4} \end{pmatrix}$ is associated with ω_i. Physically, p_a and p_o represent an average growth rate over all unstable perturbations, for each fluid.

4. Linear instability of the thermally coupled ocean-atmosphere flow: numerical results

4.1. *Numerical values of parameters for the reference case*

To represent the atmosphere and ocean, we choose the following values for our case of reference:

- Height of the atmospheric boundary layer: $H_\mathrm{a} = 1000$ m (lower turbulent part of the troposphere).
- Depth of the main thermocline: $H_\mathrm{o} = 100$ m (or thickness of the ocean mixed layer).
- Brunt-Väisälä frequency for the lower atmosphere and for the upper ocean: $N_\mathrm{a} = N_\mathrm{o} = 10^{-2}\,\mathrm{s}^{-1}$.
- Coriolis frequency: $f_0 = 10^{-4}\,\mathrm{s}^{-1}$ (common to both fluids).
- Wind speed at the top of the mixed atmospheric boundary layer: $U_1 = 15\,\mathrm{m/s}$.
- Wind speed at the interface: $U_2 = 1\,\mathrm{m/s}$.
- Oceanic current at the interface: $U_3 = 1\,\mathrm{m/s}$.
- Null oceanic speed at the main thermocline: $U_4 = 0\,\mathrm{m/s}$.
- Except for the subsection 4.2, where the coupling constants are null, we choose coupling constants: $C_\mathrm{o} = C_\mathrm{a} = 10^{-4}\ \mathrm{s}^{-1}$ (the exchanges of heat occur over a 3h time frame, which is fast; this is a strong coupling, hereafter, we will investigate the influence of the magnitude of the coupling constant).

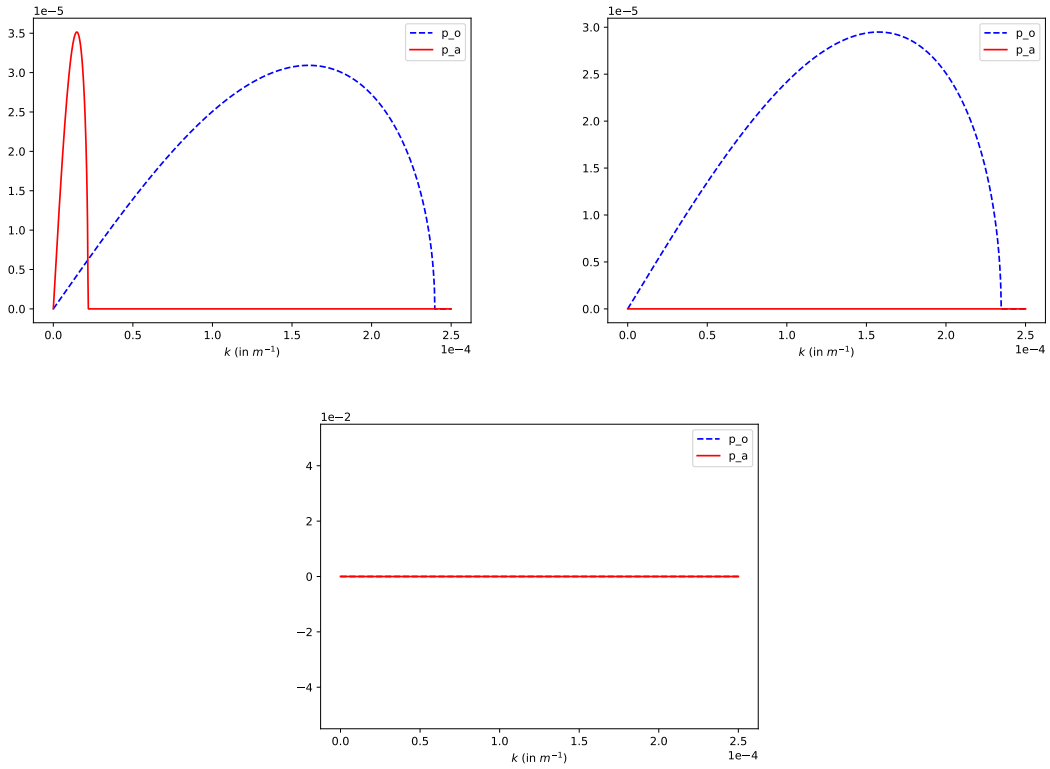

Figure 3. p_a and p_o for the reference values of the parameters, without coupling ($C_\mathrm{a} = C_\mathrm{o} = 0$) for a varying meridional wave number: $l = 10^{-5}\mathrm{m}^{-1}$ (top left panel); $l = 5 \cdot 10^{-5}\mathrm{m}^{-1}$ (top right panel); $l = 3 \cdot 10^{-4}\mathrm{m}^{-1}$ (bottom panel).

4.2. *The uncoupled case* $C_a = C_o = 0$

First, we validate our calculation of the matrix $\mathcal{A}$ by computing the instabilities for the uncoupled system (i.e. for $C_\mathrm{a} = C_\mathrm{o} = 0$). In this case, the results of the Eady model of baroclinic instability must be recovered (Eady 1949).

Remark 1 : For the uncoupled system, the matrix $\mathcal{A}$ is diagonal by block with two 2×2 real matrices, representing the atmospheric and oceanic systems. When there are instabilities in both fluids, the spectrum of $\mathcal{A}$ is then $\{\omega_1, \overline{\omega_1}, \omega_3, \overline{\omega_3}\}$, where ω_1 (resp. ω_3) represents the eigenvalues of the atmospheric (resp. oceanic) system. Then $p_\mathrm{a} = |\mathrm{Im}(\omega_1)|$ and $p_o = |\mathrm{Im}(\omega_3)|$ and only one term of the sum can be not null.

The results are shown in Figure 3. For both fluids, when l is small ($l = 10^{-5}\mathrm{m}^{-1}$, that is for 650 km wide waves), we recover the pattern of the Eady baroclinic instabilities for both fluids (Eady 1949). This is indeed observed for the whole range of zonal wavenumbers k, in the ocean and in the atmosphere. When l increases (i.e. for narrower perturbations, with a width of 130 km in panel (b) and 10 km in panel (c)), firstly the atmospheric, and then the oceanic instabilities, vanish. We recall that, in the atmosphere, the horizontal length scale of the instabilities are larger than in the ocean. This explains why increasing l suppresses atmospheric instabilities first.

4.3. *Thermally coupled system*

Now, we compute the instabilities for the coupled system with $C_\mathrm{a} = C_\mathrm{o} = 10^{-4}\,\mathrm{s}^{-1}$ (Figure 4), corresponding roughly to a 3 hours time scale for the thermal exchange between the two

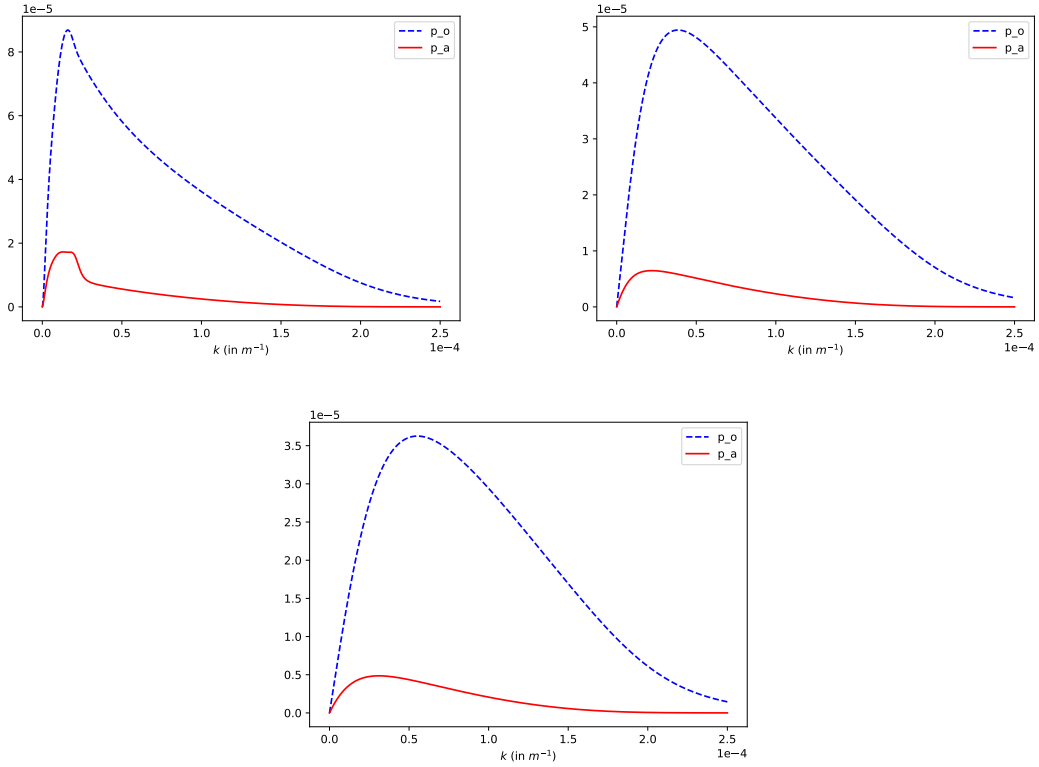

Figure 4. p_a and p_o for the coupled system, for the reference values of the parameters, with respect to k and varying l: $l = 10^{-5}\text{m}^{-1}$ (top left panel); $l = 3 \cdot 10^{-5}\text{m}^{-1}$ (top right panel); $l = 5 \cdot 10^{-5}\text{m}^{-1}$ (bottom panel); here $C_a = C_o = 10^{-4}\,\text{s}^{-1}$.

fluids, which is a strong coupling.

Comparing the uncoupled system (Figure 3) and the coupled system (Figure 4), we observe that:

- for $l = 10^{-5}\text{m}^{-1}$ (or 650 km wide waves), atmospheric perturbations are less unstable in the coupled than in the uncoupled system. For the ocean, in the coupled system, long waves are more unstable than in the uncoupled system, but short waves are less unstable. The most unstable oceanic waves have a zonal length of about 180 km. This shift in peak instability stems from coupling the oceanic waves with the long atmospheric waves. Note that, in the analytical results, we had mentioned that the coupling damps the difference between atmospheric and oceanic perturbations for very long waves.
- as l is increased (i.e. for narrower perturbations), the instability decreases in both fluids, as it does in the uncoupled system. But the instability still exists in the coupled system, whereas it had disappeared in the uncoupled flow; again, these unstable waves grow faster in the ocean than in the atmosphere. This may be related to the fact that only the thin upper layer of the ocean is considered here, while a thicker lower layer of the atmosphere is considered.
- in the ocean, the instability is shifted towards longer zonal waves and shorter meridional waves by the thermal coupling, and it does not vanish for $l = 5 \cdot 10^{-5}\text{m}^{-1}$ (width of 130 km).

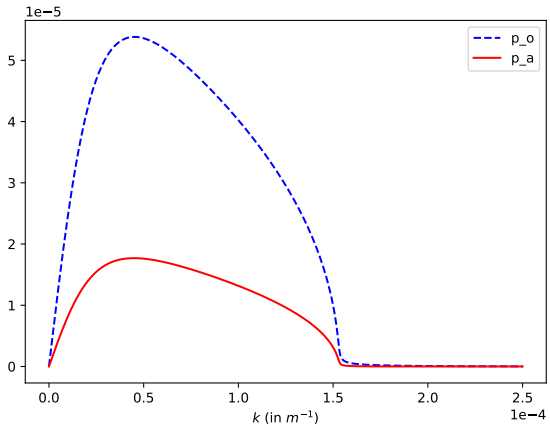

Figure 5. Instabilities for a strongly coupled system $C = 10^{-2}\,\mathrm{s}^{-1}$, for $l = 3 \cdot 10^{-5}\mathrm{m}^{-1}$

4.4. *Varying the coupling intensities*

4.4.1. *for* $l = 3 \cdot 10^{-5} m^{-1}$

In this section, we keep $l = 3 \cdot 10^{-5}\mathrm{m}^{-1}$ and the coupling intensities $\mathcal{C}_\mathrm{a}$ and C_o are varied simultaneously, with $C_\mathrm{a} = C_\mathrm{o} = C$.

Firstly, we consider a large value of C ($C = 10^{-2}\,\mathrm{s}^{-1}$, in Figure 5). In this case, the heat exchanges between the atmosphere and ocean occur on a time-scale (here, 100 seconds) very short compared to the time scales of atmospheric and oceanic instabilities (several hours or days). A remarkable fact is that the ocean and the atmosphere have an identical range of unstable zonal wavenumbers (see Figure 5). They both have a peak of instability for about 180 km long waves, zonally.
This can be understood from a qualitative analysis of the equations (12-15). When the coupling term is strong, it overcomes the terms characteristic of each fluid, which contain the mean velocity shears and buoyancy gradients. Therefore, the left-hand side of these equations, and thus the growth rates, depend more on the coupling than on the intrinsic structure of each fluid flow.
More precisely, a strong coupling tends to:

- damp the short wave instabilities and increase long wave instability for the ocean;
- decrease the long wave instabilities and favor short wave instabilities for the atmosphere.

Again this is in agreement with the asymptotic analysis provided in the previous section.

For smaller values of C (time scales for heat exchanges ranging between 5.5 hours and a day), Figure 6 shows an increase of long wave instabilities for the ocean and the atmosphere. In the case of slow heat exchanges, the instability characteristics converge towards those of the uncoupled case, for which only oceanic instabilities exist (here, for $l = 3 \cdot 10^{-5}$ m^{-1}).

4.4.2. *for* $l = 1 \cdot 10^{-5}\ m^{-1}$

In this subsection, $l = 1 \cdot 10^{-5}$ m^{-1}. We recall that for the uncoupled system (see figure 3), instabilities occur in both fluids.

Here, because atmospheric instabilities exist in the uncoupled system, we can observe (see Figure 7) that the coupling decreases the atmospheric instabilities; the atmospheric growth rates vary from $2 \cdot 10^{-5} \cdot s^{-1}$ for a high coupling to $3.5 \cdot 10^{-5} \cdot s^{-1}$ for a low coupling. The effect of the coupling on the ocean is similar to that observed in our previous analyses: the thermal coupling favors long wave oceanic instabilities that are only weakly unstable in the

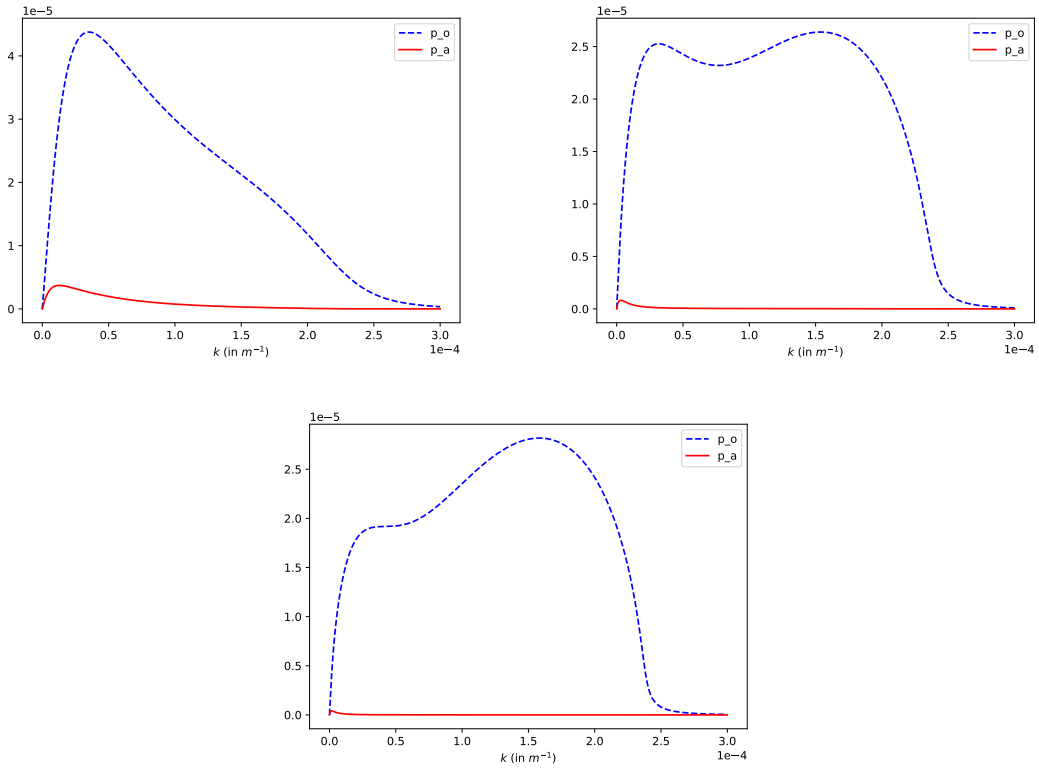

Figure 6. p_a and p_o for the coupled system, with the values of reference for the parameters, with respect to k, for $l = 3 \cdot 10^{-5}$ m^{-1} and varying C: $C = 5 \cdot 10^{-5}$s^{-1} (top left panel); $C = 1 \cdot 10^{-5}$s^{-1} (top right panel); $C = 5 \cdot 10^{-6}$s^{-1} (bottom panel).

uncoupled case.

4.5. *Varying the other parameters (H_o, H_a, U_1, U_2, U_3, U_4)*

We have carried out many tests, which are not shown here for the sake of clarity. Based on all our observations, we can conclude that a large shear ($\frac{U_1-U_2}{H_a}$ for the atmosphere and $\frac{U_3-U_4}{H_o}$ for the ocean) increases instability in the corresponding fluid and, via the coupling, can favor instability in the other fluid. Figure 8 shows two examples of this tendency.

4.6. *Remark on the vertical distribution of the instabilities*

We define, for each layer $i = 1, 2, 3, 4$:

$$p_i = \sum_{\substack{n=1 \\ \mathrm{Im}(\omega_n)>0}}^{4} \mathrm{Im}(\omega_n)|x_{n,i}|^2 \tag{40}$$

the sum of the growth rates of the instabilities, weighted by the magnitude of the eigenvectors in each layer. Then, for many cases, we note that instabilities are more intense at the top of the atmospheric boundary layer, and at the bottom of the ocean mixed layer, but not exclusively, as we can see in Figure 9. This can be understood physically as the coupling between levels 2 and 3 acts like an interfacial friction and then tends to decrease the instabilities.

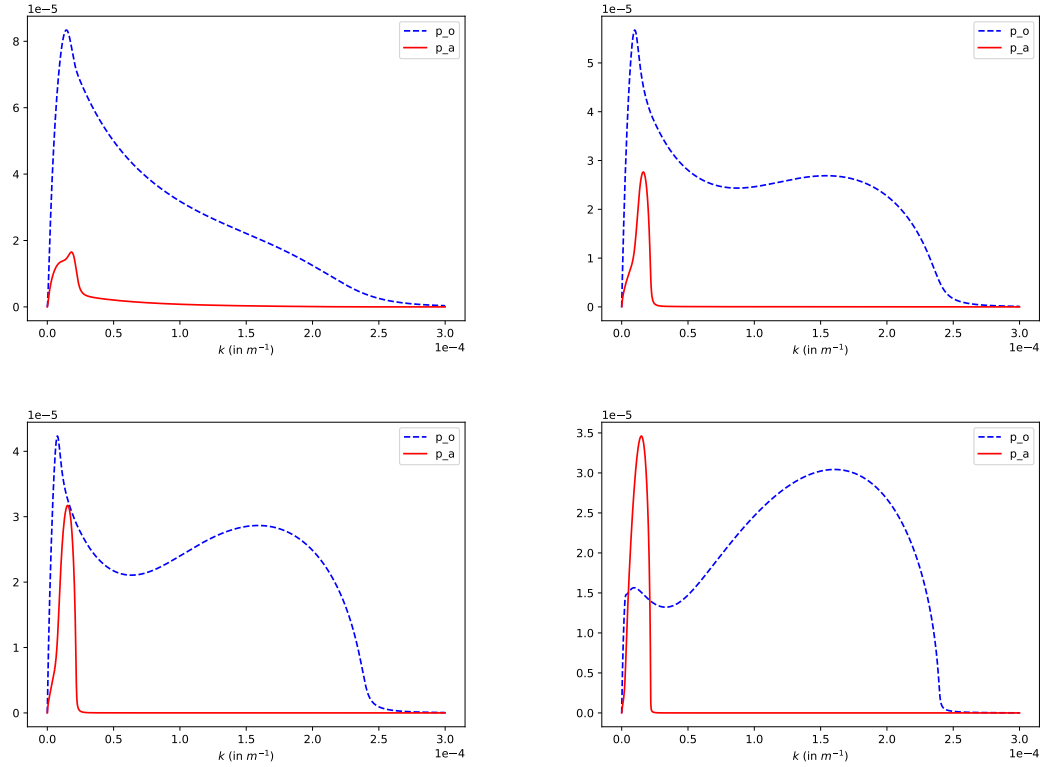

Figure 7. p_{a} and p_{o} for the coupled system, the values of reference, with respect to k, for $l = 1 \cdot 10^{-5}$ m^{-1} and varying C: $C = 5 \cdot 10^{-5}\mathrm{s}^{-1}$ (top left panel); $C = 1 \cdot 10^{-5}\mathrm{s}^{-1}$ (top right panel); $C = 5 \cdot 10^{-6}\mathrm{s}^{-1}$ (bottom left panel); $C = 1 \cdot 10^{-6}\mathrm{s}^{-1}$ (bottom right panel).

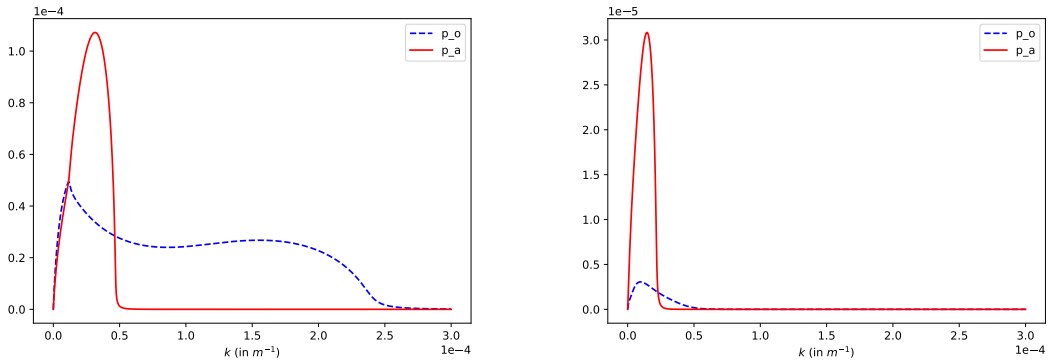

Figure 8. p_{a} and p_{o} for (left panel) a high atmospheric shear: $U_1 = 20\,\mathrm{m}$ / s and $H_{\mathrm{a}} = 500$ m and for (right panel) a low oceanic shear: $U_3 = 0.5\,\mathrm{m}$ / s and $H_{\mathrm{o}} = 500$ m. The other parameters remaining as in the reference case and $l = 1 \cdot 10^{-5}\,\mathrm{m}^{-1}$.

5. Linear instability of the mechanically coupled ocean-atmosphere flow: analytical and numerical results

Following Dewar and Flierl (1987), we derive a mechanical (stress-driven) coupling of the atmosphere and the ocean.

In a stratified quasi-geostrophic model the influence of the wind on the ocean, is achieved via the Ekman pumping (the vertical velocity due to the wind-stress curl). In a surface quasi-geostrophic model, this vertical velocity is easily introduced in the buoyancy equation for the

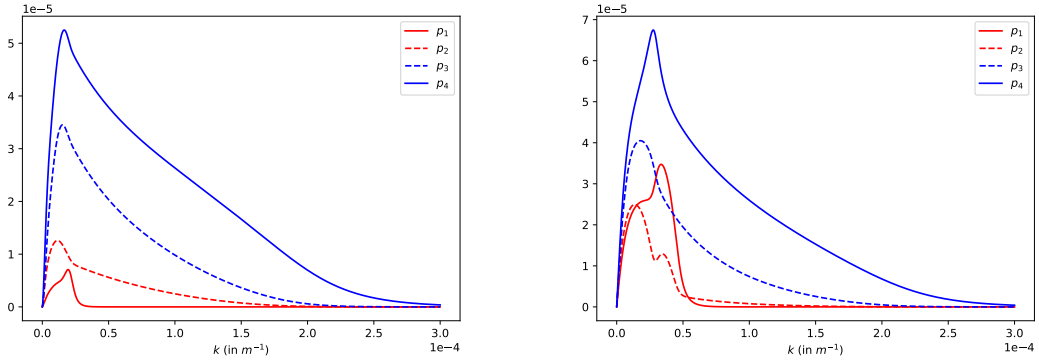

Figure 9. p_1, p_2, p_3 and p_4 for the values of reference and $l = 10^{-5}$ m^{-1} (left panel) and for a high atmospheric shear $H_\mathrm{a} = 500$ m (right panel).

ocean as:

$$\frac{\mathrm{D}b_\mathrm{o}}{\mathrm{D}t} + w_e^\mathrm{o} N_\mathrm{o}^2 = F_\mathrm{o} \tag{41}$$

where F_o is a supplementary forcing (which renders the mean flow stationary) and w_e^o is the Ekman vertical velocity for the ocean:

$$w_e^\mathrm{o} = \frac{1}{\rho_\mathrm{o} f_0}\left[\vec{\nabla}\times\vec{\tau_\mathrm{a}}\right]\cdot\vec{e_z} = \frac{1}{\rho_\mathrm{o} f_0}\left[\partial_x(\tau_\mathrm{a})_y - \partial_y(\tau_a)_x\right] \tag{42}$$

where $\vec{e_z}$ is the vertical unitary vector and $\vec{\tau_\mathrm{a}} = \begin{pmatrix}(\tau_\mathrm{a})_x\\(\tau_\mathrm{a})_y\end{pmatrix}$ is the wind stress. In a coupled model of the atmosphere and ocean, the wind stress is a quadratic function of the wind and current velocity difference:

$$\vec{\tau_\mathrm{a}} = \rho_\mathrm{a} C_d \left|\vec{u_\mathrm{a}} - \vec{u_\mathrm{o}}\right|\left(\vec{u_\mathrm{a}} - \vec{u_\mathrm{o}}\right) \tag{43}$$

where C_d is the drag coefficient and ρ_a is the density of the air. Note that when $\left|\vec{U_\mathrm{a}}\right| \gg \left|\vec{U_\mathrm{o}}\right|$, this wind stress can be linearized as

$$\vec{\tau_\mathrm{a}} = D_a\left(\vec{u_\mathrm{a}} - \vec{u_\mathrm{o}}\right)$$

where $D_a = \rho_\mathrm{a} C_d U_a$.

We assume, for our problem, that the mean flow is parallel and zonal, $V_a = V_o = 0$, as in (Dewar and Flierl 1987). We also assume that the mean oceanic and atmospheric flows are steady. In this case, the supplementary forcing exactly balances the stress exerted by each fluid on the other; for instance, for the ocean:

$$F_\mathrm{o} = \frac{N_0^2}{\rho_\mathrm{o} f_0}\left[\partial_x(\bar{\tau}_\mathrm{a})_y - \partial_y(\bar{\tau_a})_x\right]$$

with $\bar{\tau_a}$ the wind stress calculated with the mean flow U_a and U_o.
Note that, in the absence of supplementary forcing, the mean flow varies with time, and a normal mode analysis is not appropriate. A singular mode analysis must then be carried out. This is beyond the scope of the present paper. The analysis of time-varying flows, in particular periodic flows via Floquet analysis, will be the subject of a following study.

Now, we can linearize the coupled buoyancy equations around this mean flow. We have

$$\partial_t b'_\mathrm{o} + U_\mathrm{o}\partial_x b'_\mathrm{o} + v'_\mathrm{o}\partial_y B_\mathrm{o} + {w'_e}^\mathrm{o} N_\mathrm{o}^2 = 0.$$

The Ekman vertical velocity is, for the perturbation

$$w_e'^{\,\mathrm{o}} = \frac{\rho_\mathrm{a} C_d}{\rho_\mathrm{o} f_0} \left[U_\mathrm{a} - U_\mathrm{o}\right] \ \left[\partial_x (v'_\mathrm{a} - v'_\mathrm{o}) - 2\partial_y (u'_\mathrm{a} - u'_\mathrm{o})\right] \tag{44}$$

Therefore with our normal-mode perturbation, the linearized buoyancy equation with mechanical coupling, is

$$\partial_t b'_\mathrm{o} + U_\mathrm{o}\partial_x b'_\mathrm{o} + v'_\mathrm{o}\partial_y B_\mathrm{o} = -\frac{\rho_\mathrm{a} C_d N_\mathrm{o}^2}{\rho_\mathrm{o} f_0} \left(k^2 + 2l^2\right) \left[\psi'_\mathrm{a} - \psi'_\mathrm{o}\right] \ \left[U_\mathrm{a} - U_\mathrm{o}\right] \tag{45}$$

at the ocean surface (layer 3), and

$$\partial_t b'_\mathrm{o} + U_\mathrm{o}\partial_x b'_\mathrm{o} + v'_\mathrm{o}\partial_y B_\mathrm{o} = 0 \tag{46}$$

at the ocean bottom (layer 4), and conversely for the atmosphere, in which the "a" and "o" indices in the formulae above must be permuted.
Now the variables are Fourier decomposed and the equations are divided by ik; this provides a pure imaginary coupling of the perturbation equations, as for the thermal coupling. Finally we have to solve the following matrix equation: $\mathcal{M}\beta = 0$ where

$$\mathcal{M} = \begin{pmatrix} \omega - k\left(\Pi_\mathrm{a} + \Lambda_\mathrm{a}\left(H_\mathrm{a} - \frac{f_0}{t_\mathrm{a}}\right)\right) & \frac{-f_0 k \Lambda_\mathrm{a}}{s_\mathrm{a}} & 0 & 0 \\ \frac{f_0 k \Lambda_\mathrm{a}}{s_\mathrm{a}} - \frac{\mathrm{iMC_o}}{s_\mathrm{a}} & \omega - k\left(\Pi_a + \frac{f_0 \Lambda_\mathrm{a}}{t_\mathrm{a}}\right) + \frac{\mathrm{iMC_o}}{t_\mathrm{a}} & \frac{\mathrm{iMC_o}}{t_\mathrm{o}} & -\frac{\mathrm{iMC_o}}{s_\mathrm{o}} \\ -\frac{\mathrm{iMC_a}}{s_\mathrm{a}} & \frac{\mathrm{iMC_a}}{t_\mathrm{a}} & \omega - k\left(\Pi_\mathrm{o} - \frac{f_0 \Lambda_\mathrm{o}}{t_\mathrm{o}}\right) + \frac{\mathrm{iMC_a}}{t_\mathrm{o}} & -\frac{f_0 k \Lambda_\mathrm{o}}{s_\mathrm{o}} - \frac{\mathrm{iMC_a}}{s_\mathrm{o}} \\ 0 & 0 & \frac{f_0 k \Lambda_\mathrm{o}}{s_\mathrm{o}} & \omega - k\left(\Pi_\mathrm{o} + \Lambda_\mathrm{o}\left(\frac{f_0}{t_\mathrm{o}} - H_\mathrm{o}\right)\right) \end{pmatrix} \tag{47}$$

where $\mathrm{MC_a} = -\mathrm{MC_o} = -\frac{\rho_\mathrm{a} C_d N_\mathrm{o}^2}{\rho_\mathrm{o} f_0}\left(k^2 + 2l^2\right)\left[U_2 - U_3\right]$ are the mechanical coupling coefficients. This is equivalent to find the eigenvalues of the matrix $\mathcal{A}$ where

$$\mathcal{A} = \begin{pmatrix} k\left(\Pi_\mathrm{a} + \Lambda_\mathrm{a}\left(H_\mathrm{a} - \frac{f_0}{t_\mathrm{a}}\right)\right) & \frac{f_0 k \Lambda_\mathrm{a}}{s_\mathrm{a}} & 0 & 0 \\ -\frac{f_0 k \Lambda_\mathrm{a}}{s_\mathrm{a}} + \frac{\mathrm{iMC_o}}{s_\mathrm{a}} & k\left(\Pi_a + \frac{f_0 \Lambda_\mathrm{a}}{t_\mathrm{a}}\right) - \frac{\mathrm{iMC_o}}{t_\mathrm{a}} & -\frac{\mathrm{iMC_o}}{t_\mathrm{o}} & \frac{\mathrm{iMC_o}}{s_\mathrm{o}} \\ \frac{\mathrm{iMC_a}}{s_\mathrm{a}} & -\frac{\mathrm{iMC_a}}{t_\mathrm{a}} & k\left(\Pi_\mathrm{o} - \frac{f_0 \Lambda_\mathrm{o}}{t_\mathrm{o}}\right) - \frac{\mathrm{iMC_a}}{t_\mathrm{o}} & \frac{f_0 k \Lambda_\mathrm{o}}{s_\mathrm{o}} + \frac{\mathrm{iMC_a}}{s_\mathrm{o}} \\ 0 & 0 & -\frac{f_0 k \Lambda_\mathrm{o}}{s_\mathrm{o}} & k\left(\Pi_\mathrm{o} + \Lambda_\mathrm{o}\left(\frac{f_0}{t_\mathrm{o}} - H_\mathrm{o}\right)\right) \end{pmatrix} \tag{48}$$

5.1. *Asymptotic limit for long zonal waves* $k \to 0$ *and finite width perturbations* $l \neq 0$

The determinant of $\mathcal{M}$ can easily be computes for long zonal waves $k \to 0$ with finite meridional scale $l \neq 0$: the matrix $\mathcal{M}$ becomes

$$\lim_{k\to 0} \mathcal{M} = \begin{pmatrix} \omega & 0 & 0 & 0 \\ -\frac{\widetilde{\mathrm{iMC_o}}}{\widetilde{s_\mathrm{a}}} & \omega + \frac{\widetilde{\mathrm{iMC_o}}}{\widetilde{t_\mathrm{a}}} & \frac{\widetilde{\mathrm{iMC_o}}}{\widetilde{t_\mathrm{o}}} & -\frac{\widetilde{\mathrm{iMC_o}}}{\widetilde{s_\mathrm{o}}} \\ -\frac{\widetilde{\mathrm{iMC_a}}}{\widetilde{s_\mathrm{a}}} & \frac{\widetilde{\mathrm{iMC_a}}}{\widetilde{t_\mathrm{a}}} & \omega + \frac{\widetilde{\mathrm{iMC_a}}}{\widetilde{t_\mathrm{o}}} & -\frac{\widetilde{\mathrm{iMC_a}}}{\widetilde{s_\mathrm{o}}} \\ 0 & 0 & 0 & \omega \end{pmatrix} \tag{49}$$

where $\widetilde{\mathrm{MC}_j} = \lim_{k\to 0} \mathrm{MC}_j = \pm\frac{2\rho_\mathrm{a} C_d N_\mathrm{o}^2 l^2}{\rho_\mathrm{o} f_0}\left[U_2 - U_3\right]$, $\widetilde{s_j} = \lim_{k\to 0} s_j = N_j l \sinh\left(\frac{N_j}{f_0} l H_j\right)$ and $\widetilde{t_j} = \lim_{k\to 0} t_j = N_j l \tanh\left(\frac{N_j}{f_0} l H_j\right)$ for $j = \mathrm{a}, \mathrm{o}$. A pure imaginary solution to $\det\left(\lim_{k\to 0}\mathcal{M}\right)$ is

$$-\mathrm{i}\left[\frac{\widetilde{\mathrm{MC_o}}}{\widetilde{t_\mathrm{a}}} + \frac{\widetilde{\mathrm{MC_a}}}{\widetilde{t_\mathrm{o}}}\right] < 0 \tag{50}$$

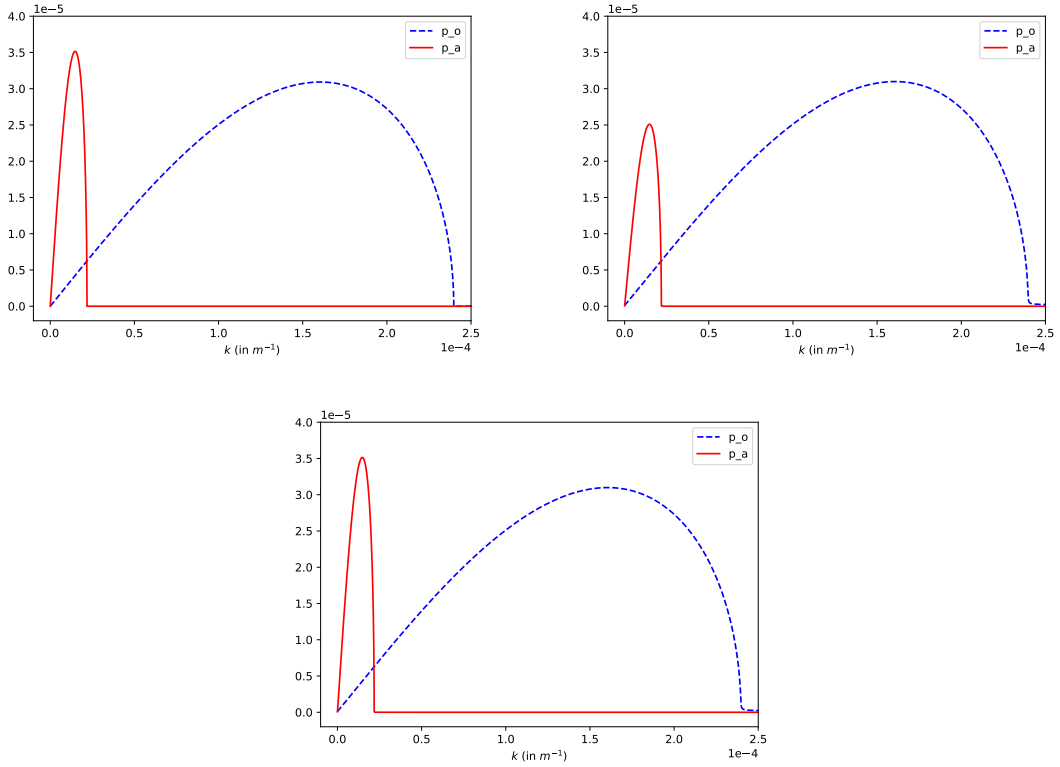

Figure 10. p_a and p_o for the values of reference and $l = 10^{-5}$ m^{-1}. The upper left panel is for $U_2 = 1$ m / s (no mechanical coupling) and the upper right panel is for $U_2 = 5$ m / s. The bottom panel is for $U_1 = 19$ m / s and $U_2 = 5$ m / s (same Λ_a as for the no coupled case).

So the coupling tends to destabilize the system for long zonal waves. But because $\widetilde{\mathrm{MC}_j} \to 0$ as $l \to 0$, the destabilization are weaker as $K \to 0$.

We have run these equations for parameters characteristic of the ocean and atmosphere at the same scales as for the thermal coupling (see subsection 4.1). The effect of the mechanical coupling appeared weak for the situations considered. Figure 10 shows that the key element for the instability in both fluids is the local vertical shear of velocity. Figure 11) shows that the mechanical coupling has an effect only for very large drag coefficients, favoring the growth of short-scale perturbations.

6. Discussion

This study of the linear instability growth rates of a thermally coupled four-layer SQG model shows several differences from the classical uncoupled Eady model:

- The long-wave atmospheric instabilities are damped. Conversely, the long waves oceanic instabilities are enhanced for a thermally coupled Eady model.
- The short-wave atmospheric instabilities appear in the coupled model, since they do not exist in the classical Eady model. They appear due to the presence of short-wave oceanic instabilities, but are damped by the coupling.
- The system is continuous with respect to the coupling: very small coupling terms tend towards the uncoupled case.

The mechanical coupling of the two Eady systems lead to a weak modification of their

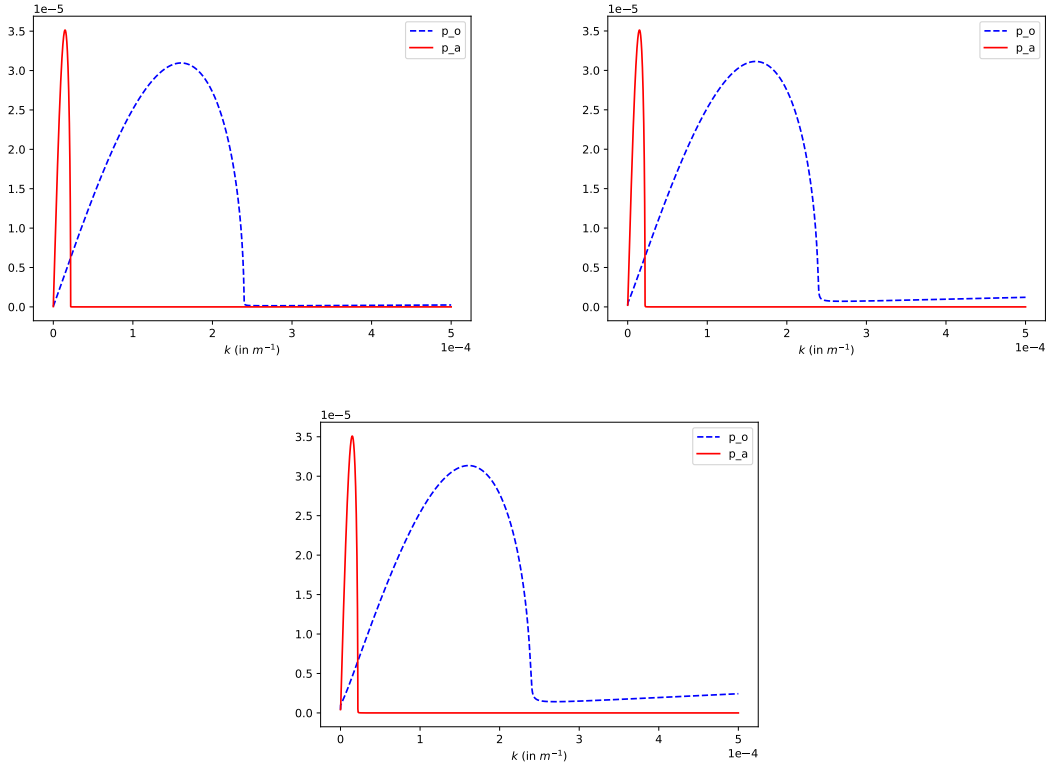

Figure 11. p_a and p_o for the values of reference and $l = 10^{-5}$ m^{-1}. The varying parameter here is the drag coefficient C_d: $C_d = 1 \cdot 10^{-3}, 5 \cdot 10^{-3}, 1 \cdot 10^{-2}$, from top left to bottom (knowing that a realistic value for C_d is around $1.5 \cdot 10^{-3}$).

stability properties in the limit of our parameter ranges. Short waves are slightly destabilized in the ocean.

The main difference between this work and the previous ones in the literature is that in Renault *et al.* (2016, 2017, 2018) they essentially consider the wind coupling with oceanic vortices. The instability of the wind or of the vortices was not included in their model.

7. Conclusions

The framework of the present study was purposefully limited to allow analytical computations, and to prevent too large a parameter sensitivity study. The present work does not claim to represent a real ocean coupled to the atmosphere, but provides hints about the unstable regimes for various sets of physical parameters. Among the limitations of the model, an important one is the reduction to only four levels of flow and zero potential vorticity inside each fluid: the flow is essentially geostrophic and the model does not allow for horizontal shear (barotropic) instability (here U_1, U_2, U_3, U_4 do not depend on y). The study of barotropic instabilities could be achieved in a simpler model with one atmospheric layer coupled to one oceanic layer. Also, the present model does not allow vertical velocities (i.e. vertical fluxes of heat) nor radiative fluxes. They should be added in a sequel of this work. As mentionned above, the steadiness of the mean flow is also a limitation, and a following study will investigate time-periodic mean flows.

Another interesting case is the coupling of a zonal wind with a circular oceanic vortex. Unfortunately, it cannot be adressed analytically due to the geometrical constraints, as it

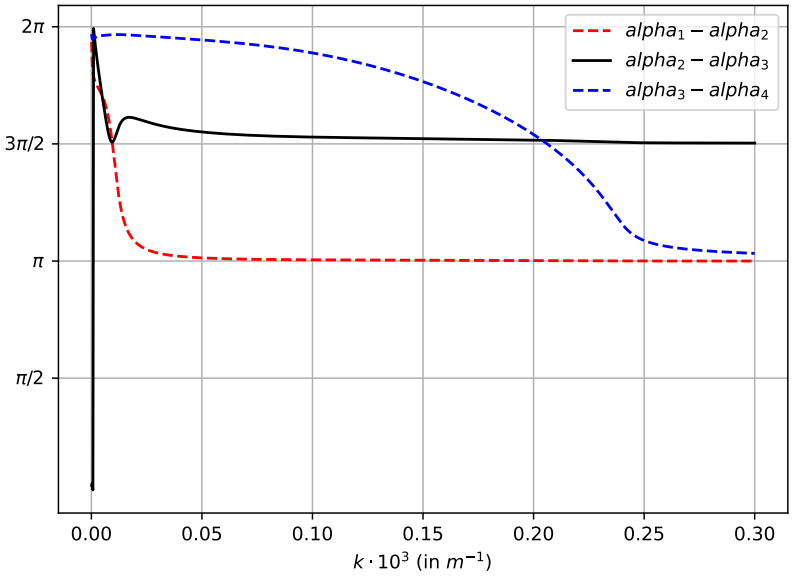

Figure A1. Phase shift for the thermal coupling. The parameters are at their values of reference (see section 4.1), $l = 10^{-5}\mathrm{m}^{-1}$, $C_\mathrm{a} = C_\mathrm{o} = 10^{-5}\mathrm{s}^{-1}$.

would mix polar and Cartesian coordinates. However, it will be solved numerically in a coupled SQG model and proposed in a subsequent paper. These studies will then be extended to a 3D primitive equation model.

Appendix A: Phase shifts of the instabilities

An analysis of the perturbation phase shifts can explain why the instabilities cannot grow in the mechanically coupled model: from the eigenvector corresponding to the largest growth rate of the whole system $\beta = \begin{pmatrix} \beta_1 \\ \beta_2 \\ \beta_3 \\ \beta_4 \end{pmatrix}$, we compute the phase of the unstable wave in each layer: $\alpha_i = \arg(\beta_i)$. Figure A1 (respectively Figure A2) shows the phase shift between successive levels for the thermally (respectively mechanically) coupled model.

Firstly, inside each fluid, for both couplings, the structure is similar: the perturbations are phased (the dephasing is 2π) for small k and the phase shift decreases with k to reach π (the perturbations are in opposition of phase) for the values of k where the fluid becomes stable (around $0.03 \cdot 10^{-3}\mathrm{m}^{-1}$ for the atmosphere and around $0.25 \cdot 10^{-3}\mathrm{m}^{-1}$ for the ocean).
Secondly, at the interface, the structure is different for the thermal or mechanical couplings. For $k < 0.02 \cdot 10^{-3}\mathrm{m}^{-1}$, the phase shift of the perturbations at the interface lies between $3\pi/2$ and 2π for the thermal coupling (the atmospheric perturbation is delayed with respect to the oceanic one). For the mechanical coupling and the same range of k, the phase shift is slightly larger than $\pi/2$: thus, the oceanic perturbation is delayed with respect to the atmospheric one. This explains why the mechanical coupling damps the instabilities: it forces a delay of oceanic waves with respect to atmospheric waves (thanks to the friction modeled in the mechanical coupling), whereas a phase shift between $3\pi/2$ and 2π (as for the thermal coupling) is favorable

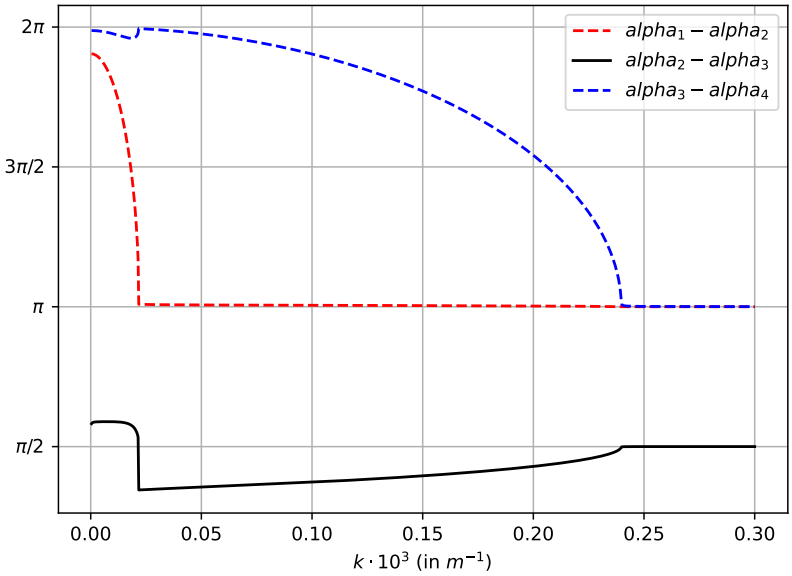

Figure A2. Phase shift for the mechanical coupling. The parameters are at their values of reference (see section 4.1), $l = 10^{-5}\mathrm{m}^{-1}$, $C_d = 2 \cdot 10^{-3}$.

to the instability.

References

Bjerkness, J., A possible response of the atmospheric Hadley circulation to equatorial anomalies of ocean temperature. *Tellus*, 1966, **18**, 820–829.

Bretherton, F.P., Critical layer instability in baroclinic flows. *Q. J. R. Meteorol. Soc.*, 1966, **92**, 325–334.

Carton, X., Instability of Surface Quasigeostrophic Vortices. *J. Atmos. Sci.*, 2009, **66**, 1051–1062.

Carton, X.J., Hydrodynamical modelling of oceanic vortices. *Surv. Geophys.*, 2001, **22**, 179–263.

Carton, X.J., Oceanic Vortices; in *Fronts, Waves and Vortices in Geophysical Flows*, edited by J.B. Flor, Vol. Lecture Notes in Physics, 805, 2010, pp. 61–108.

Chelton, D.B. and Xie, S.P., Coupled ocean-atmosphere interaction at oceanic mesoscales. *Oceanography*, 2010, **23**, 52–69.

Dewar, W.K. and Flierl, G.R., Some Effects of the Wind on Rings. *J. Phys. Oceanogr.*, 1987, **17**, 1653—-1667.

Duarte, R.M., Carton, X.J., Capet, X. and Cherubin, L., Trapped Instability and Vortex Formation by an Unstable Coastal Current. *Reg. Chaot. Dyn.*, 2011, **16**, 577–601.

Duarte, R.M., Carton, X.J. and Poulin, F.J., The dynamics of a meandering coastal jet in the lee of a cape. *Reg. Chaot. Dyn.*, 2016, **21**, 274–290.

Eady, E.T., Long Waves and Cyclone Waves. *Tellus*, 1949, **1**, 33–52.

Fernández-Castro, B., Evans, D.G., Frajka-Williams, E., Vic, C. and Naveira-Garabato, A.C., Breaking of Internal Waves and Turbulent Dissipation in an Anticyclonic Mode Water Eddy. *J. Phys. Oceanogr.*, 2020, **50**, 1893–1914.

Fofonoff, N.P., The Gulf-Stream; in *Evolution of Physical Oceanography: scientific surveys in honor of Henry Stommel*, 1981, pp. 112–139.

Gula, J., Taylor, J., Shcherbina, A. and Mahadevan, A., Submesoscale processes and Mixing. In *Ocean Mixing: Drivers, Mechanisms and Impacts*, pp. 181–214, 2022 (Elsevier BV: ????).

Held, I., PierreHumbert, R.T., Garner, S.T. and Swanson, K.L., Surface quasi-geostrophic dynamics. *J. Fluid Mech.*, 1995, pp. 1–20.

Holland, W.R. and Haidvogel, D.B., A parameter study of the mixed instability of idealized ocean currents. *Dyn. Atmos. Oceans*, 1980, **4**, 185–215.

Lapeyre, G., Surface Quasi-Geostrophy. *Fluids*, 2017, **2**, 1–28.

McCreary, J.P., A Model of Tropical Ocean-Atmosphere Interaction. *Mon. Weather Rev.*, 1983, **111**, 370–387.

McWilliams, J.C., Submesoscale currents in the ocean. *Proc. R. Soc. A*, 2016, **472**.

Meunier, T., Carton, X.J. and Duarte, R., Influence of a deep flow on a surface boundary current. *Geophys. Astrophys. Fluid Dyn.*, 2013, **107**, 277–303.

Nowlin, W.D. and Klinck, J.M., The physics of the Antarctic Circumpolar Current. *Rev. Geophys.*, 1986, **24**, 469–491.

Renault, L., Marchesiello, P., Masson, S. and McWilliams, J.C., Remarkable Control of Western Boundary Currents by Eddy Killing, a Mechanical Air-Sea Coupling Process. *Geophys. Res. Lett.*, 2017, **46**, 2743–2751.

Renault, L., McWilliams, J.C. and Gula, J., Dampening of Submesoscale Currents by Air-Sea Stress Coupling in the Californian Upwelling System. *Sci. Rep.*, 2018, **8**, 1–7.

Renault, L., Molemaker, J.M., McWilliams, J.C., Shchepetkin, A.F., Lemarié, F., Chelton, D., Illig, S. and Hall, A., Modulation of Wind Work by Oceanic Current Interaction with the Atmosphere. *J. Phys. Oceanogr.*, 2016, **46**, 1685–1704.

Richardson, P.L., Gulf-Stream rings; in *Eddies in Marine Science*, edited by A.R. Robinson, Vol. Topics in Atmospheric and Oceanographic Sciences, 1983, pp. 19–45.

Stevens, B., Bony, S., Farrell, D., Ament, F., Blyth, A., Fairall, C., Karstensen, J., Quinn, P.K., Speich, S., Acquistapace, C., Aemisegger, F., Albright, A.L., Bellenger, H., Bodenschatz, E., Caesar, K.A., Chewitt-Lucas, R., de Boer, G., Delanoë, J., Denby, L., Ewald, F., Fildier, B., Forde, M., George, G., Gross, S., Hagen, M., Hausold, A., Heywood, K.J., Hirsch, L., Jacob, M., Jansen, F., Kinne, S., Klocke, D., Kölling, T., Konow, H., Lothon, M., Mohr, W., Naumann, A.K., Nuijens, L., Olivier, L., Pincus, R., Pöhlker, M., Reverdin, G., Roberts, G., Schnitt, S., Schulz, H., Siebesma, A.P., Stephan, C.C., Sullivan, P., Touzé-Peiffer, L., Vial, J., Vogel, R., Zuidema, P., Alexander, N., Alves, L., Arixi, S., Asmath, H., Bagheri, G., Baier, K., Bailey, A., Baranowski, D., Baron, A., Barrau, S., Barrett, P.A., Batier, F., Behrendt, A., Bendinger, A., Beucher, F., Bigorre, S., Blades, E., Blossey, P., Bock, O., Böing, S., Bosser, P., Bourras, D., Bouruet-Aubertot, P., Bower, K., Branellec, P., Branger, H., Brennek, M., Brewer, A., Brilouet, P.E., Brügmann, B., Buehler, S.A., Burke, E., Burton, R., Calmer, R., Canonici, J.C., Carton, X., Cato Jr., G., Charles, J.A., Chazette, P., Chen, Y., Chilinski, M.T., Choularton, T., Chuang, P., Clarke, S., Coe, H., Cornet, C., Coutris, P., Couvreux, F., Crewell, S., Cronin, T., Cui, Z., Cuypers, Y., Daley, A., Damerell, G.M., Dauhut, T., Deneke, H., Desbios, J.P., Dörner, S., Donner, S., Douet, V., Drushka, K., Dütsch, M., Ehrlich, A., Emanuel, K., Emmanouilidis, A., Etienne, J.C., Etienne-Leblanc, S., Faure, G., Feingold, G., Ferrero, L., Fix, A., Flamant, C., Flatau, P.J., Foltz, G.R., Forster, L., Furtuna, I., Gadian, A., Galewsky, J., Gallagher, M., Gallimore, P., Gaston, C., Gentemann, C., Geyskens, N., Giez, A., Gollop, J., Gouirand, I., Gourbeyre, C., de Graaf, D., de Groot, G.E., Grosz, R., Güttler, J., Gutleben, M., Hall, K., Harris, G., Helfer, K.C., Henze, D., Herbert, C., Holanda, B., Ibanez-Landeta, A., Intrieri, J., Iyer, S., Julien, F., Kalesse, H., Kazil, J., Kellman, A., Kidane, A.T., Kirchner, U., Klingebiel, M., Körner, M., Kremper, L.A., Kretzschmar, J., Krüger, O., Kumala, W., Kurz, A., L'Hégaret, P., Labaste, M., Lachlan-Cope, T., Laing, A., Landschützer, P., Lang, T., Lange, D., Lange, I., Laplace, C., Lavik, G., Laxenaire, R., Le Bihan, C., Leandro, M., Lefevre, N., Lena, M., Lenschow, D., Li, Q., Lloyd, G., Los, S., Losi, N., Lovell, O., Luneau, C., Makuch, P., Malinowski, S., Manta, G., Marinou, E., Marsden, N., Masson, S., Maury, N., Mayer, B., Mayers-Als, M., Mazel, C., McGeary, W., McWilliams, J.C., Mech, M., Mehlmann, M., Meroni, A.N., Mieslinger, T., Minikin, A., Minnett, P., Möller, G., Morfa Avalos, Y., Muller, C., Musat, I., Napoli, A., Neuberger, A., Noisel, C., Noone, D., Nordsiek, F., Nowak, J.L., Oswald, L., Parker, D.J., Peck, C., Person, R., Philippi, M., Plueddemann, A., Pöhlker, C., Pörtge, V., Pöschl, U., Pologne, L., Posyniak, M., Prange, M., Quiñones Meléndez, E., Radtke, J., Ramage, K., Reimann, J., Renault, L., Reus, K., Reyes, A., Ribbe, J., Ringel, M., Ritschel, M., Rocha, C.B., Rochetin, N., Röttenbacher, J., Rollo, C., Royer, H., Sadoulet, P., Saffin, L., Sandiford, S., Sandu, I., Schäfer, M., Schemann, V., Schirmacher, I., Schlenczek, O., Schmidt, J., Schröder, M., Schwarzenboeck, A., Sealy, A., Senff, C.J., Serikov, I., Shohan, S., Siddle, E., Smirnov, A., Späth, F., Spooner, B., Stolla, M.K., Szkółka, W., de Szoeke, S.P., Tarot, S., Tetoni, E., Thompson, E., Thomson, J., Tomassini, L., Totems, J., Ubele, A.A., Villiger, L., von Arx, J., Wagner, T., Walther, A., Webber, B., Wendisch, M., Whitehall, S., Wiltshire, A., Wing, A.A., Wirth, M., Wiskandt, J., Wolf, K., Worbes, L., Wright, E., Wulfmeyer, V., Young, S., Zhang, C., Zhang, D., Ziemen, F., Zinner, T. and Zöger, M., EUREC^{4}A. *Earth Syst. Sci. Data*, 2021, **13**, 4067–4119.

Tulloch, R., Marshall, J., Hill, C. and Smith, K.S., Scales, Growth Rates, and Spectral Fluxes of Baroclinic Instability in the Ocean. *J. Phys. Oceanogr.*, 2011, **41**, 1057–1076.

Vic, A., Carton, X. and Gula, J., The Interaction of Two Unsteady Point Vortex Sources in a Deformation Field in 2D Incompressible Flows. *Reg. Chaot. Dyn.*, 2021, **26**, 618–646.